NASA Contractor Report 3836

NASA-CR-3836 19850003700

Inverse Design Technique for Cascades

Luca Zannetti and Maurizio Pandolfi

NASA

NASA Contractor Report 3836

Inverse Design Technique
for Cascades

Luca Zannetti and Maurizio Pandolfi
G.M.A.F., Inc.
Freeport, New York

NΛSΛ
National Aeronautics
and Space Administration

Scientific and Technical
Information Branch

1984

INTRODUCTION

This report describes a methodology to solve the inverse design problem for cascades of airfoils, assuming the flow to be two-dimensional and the gas inviscid, compressible and ideal. The methodology is based on the procedure described in [1] for the computation of transonic nozzle and plume flows, in [2] for the solution of the inverse problem in channels, and in [3] for the inverse cascade problem.

The basic idea is the following. A time-dependent computation is performed, where a distribution of pressure is prescribed on a wall, the geometry of which is unknown and has to be determined. Such a wall is a boundary of the flow field and it is assumed as a flexible and impermeable surface. If the flow tends to produce a pressure on the wall, different from the one which was prescribed, the wall itself will move, adjusting its shape, until any mismatching is eliminated.

The inverse problem may be formulated in different ways, both for airfoils and cascades. Such differences stem from a choice of possible prescriptions, such as the shape of the camber line, the thickness and/or lift distribution along the camber line, the pressure distribution on a single side of the profile, and also on the boundary condition assumed in front of it and behind it [3].

In Section 1 we report the methodology for the design of a cascade of airfoils, under the following upstream and downstream boundary conditions. Total pressure, total temperature and flow angle are imposed upstream. The static pressure is prescribed downstream. We describe the numerical technique, showing in detail how moving boundaries are treated for different formulations of the inverse problem. Numerical examples are presented for wholly subsonic flows and also for the design of shockless blades in the transonic regime. The section ends with an attempt to predict a specific shockless cascade designed by Hobson [4], by prescribing the thickness and lift distribution along the camber line. The method, as described in Section 1, fails to produce the expected solution.

An analysis of the causes of such a failure is developed in Section 2. Global considerations, relating upstream and downstream boundary conditions with the prescribed distribution of flow properties on the profile show that some geometries (such as the Hobson cascade) cannot be predicted by the methodology, unless different

conditions are imposed at the downstream boundary.

In Section 3 the actual two-dimensional problem is reformulated in a one-dimensional approximation, introducing a suitable force field. Simple numerical experiments are performed to validate the conclusions of Section 2. A different treatment of downstream boundary conditions is proposed, as a possible way for overcoming the difficulties encountered with the Hobson cascade. Actual applications of the concept to the two-dimensional problem will be discussed in a forthcoming Report.

In Section 4 we present an extension of the method to the design of high-staggered cascades. When the stagger is high, the computational grid described in Section 1 tends to depart too much from an orthogonal pattern, and accuracy can be impaired. A modified H-grid is then introduced, together with proper definitions of upstream and downstream boundary conditions. The Section ends with a presentation of numerical results.

1. GENERAL FORMULATION OF THE PROBLEM

For a cascade of airfoils, the inverse problem consists of finding the geometry of a cascade producing a flow of which some parameters are prescribed. There is a certain freedom in the formulation of the problem. For example, in addition to suitable conditions at infinity, one may:

i) prescribe the distribution of thickness and pressure jump along the chord of a profile, and inquire for the geometry of the camber line,

ii) prescribe the distribution of thickness and pressure on one side of the profile, and again inquire for the geometry of the camber line, or

iii) prescribe the pressure distribution around the profile and inquire for its geometry.

Novak and Haymann-Haber [5] have given a solution to problem i), based on the Taylor expansion of the equations of the steady motion for a compressible inviscid flow. As they point out, such a procedure may fail if stagnation points are in the flow field. We will begin by solving Novak's problem by a different technique. Therefore, we will consider profiles having sharp leading edges and we will assume that there are no stagnation points. Our technique, however, allows more general problems to be solved, where the profiles have blunt leading edges, provided that the problem be split into two parts. On a small portion of the profile around the leading edge, the geometry of the profile is prescribed. The geometry of the rest of the profile will be determined to satisfy one of the sets of conditions mentioned above. Consequently, the stagnation point will find its proper location through a direct analysis of the leading edge region. The price to be paid is a more complicated mapping

needed to describe the leading edge region.

The numerical technique described in the present paper follows the outlines described in [1] for the computation of transonic nozzle and plume flows, and in [2] for the solution of the inverse problem in channels. Briefly, a time-dependent computation is performed, in which the boundary conditions are imposed according to the formulation of the inverse problem, until a steady state is reached asymptotically. The contours of the blades are considered as impermeable but perfectly deformable. An initial geometry is assumed. Since such a geometry is incompatible with a steady motion, consistent with the prescribed conditions, a transient is generated. During the transient, the walls of the blades change in shape, in order to satisfy the condition of impenetrability as well as the boundary conditions, compatible with problem i), ii), or iii) above. The solution of the inverse problem is given by the geometry obtained asymptotically.

The method of solution, thus, consists of a numerical description of a physical evolution in time. The partial differential equations of motion are discretized as finite difference equations. Mathematically, the problem is a mixed initial-and-boundary-value hyperbolic problem. Since the publication of [2], remarkable progress has been made in the numerical treatment of such problems, both in integration schemes and in the calculation of boundaries. Our present numerical scheme is consistent with the propagation of waves as implicitly described by the Euler equations of motion. It belongs to the λ-family; details can be found in Refs. 6 through 9. in brief, the finite difference scheme is based on the use of one-sided differences, according to the direction of propagation of signals along the bicharacteristics in a transient, preserving the domain of dependence of each computed point. The main advantages of this technique are its robustness and consistency with the physical phenomena. The accuracy is good even with coarse meshes and in regions where the gradients of the flow properties are strong or transonic transitions occur. Furthermore, the treatment of the boundaries, which is crucial in this type of problems, is simple and naturally consistent with the treatment of inner points, as well as with the overall physical phenomenon to be described.

For simplicity, the inverse problem is studied here under the assumption that the flow is irrotational and two-dimensional. Three-dimensional problems are only more complicated from a formal point of view. Straightforward extensions of the general technique to rotational flows have already been made [8].

Other approaches to the inverse problem, similar in some aspects to the one proposed here, have been developed independently in Refs. 10 and 11. However, the formulations of the problem are different from the present one and the methods proposed seem to converge to a solution only if the initial configuration is very close to the solu-

tion itself.

A very important point has to be discussed when dealing with in-
verse problems: the well-posedness of the problem itself. Problem
iii) is discussed in the case of a single airfoil in [12], where it
is shown that the design data cannot be prescribed with complete
freedom. In fact, they must satisfy some constraints which are dic-
tated by the consistency of the data with the flow conditions at in-
finity and by the requirement that the contour of the airfoil must be
closed. The number of constraints depends on the way the inverse
problem is formulated. This matter is analytically clear for in-
compressible potential flow [13, 14]. Unfortunately, there is not an
exhaustive theory capable of prescribing the constraints that lead to
a well-posed problem for compressible flow. In [12] a way is provid-
ed to circumvent such difficulties, but the suggestion given there
cannot be applied to the present cases, due to the peculiar formula-
tion of the inverse problems. We address the subject with a dif-
ferent attitude. We use a "physical" time-dependent technique. If
the design data which we impose violate the constraints needed by the
"steady" well-posed problem, we expect the computation never to be-
come steady. Moreover, the well-posedness of a time-dependent formu-
lation also depends on the upstream and downstream boundary condi-
tions, as discussed in [15]. In fact, instabilities can be generated
by upstream and/or downstream conditions that, together with the con-
ditions prescribed along the blade surfaces, do not allow the flow to
get stabilized but, on the contrary, amplify its unsteadiness until
the computation blows up. In particular, one of the main goals of
the present paper is to show how, having prescribed a certain down-
stream pressure, there are two possible solutions to problem i), only
one of which is stable from the viewpoint of a time-dependent tech-
nique.

Formulation ii) also presents an ambiguous feature which should
be discussed. When the pressure distribution is prescribed on one
side of the blade, together with its thickness, it cannot be said a
priori whether that side has to play the role of a suction side or of
a pressure side. The computation itself will select the role of the
side on which the pressure distribution has been assigned. According
to our numerical results, the computation selects that side as the
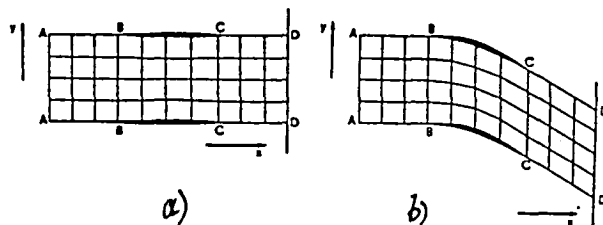pressure side.

Fig. 1.1

1.1 The physical problem

We proceed now to describe the physical process which we have chosen to generate the solution. Figs. 1.1 a) and 1.1 b) show typical initial and final configurations. The flow is assumed to be confined between two consecutive blades, the arcs BC, and two parallel lines issuing from the leading edge and the trailing edge of the blades. The lines in front of the blades are denoted by AB. The lines behind the blades are denoted by CD. Such boundaries are assumed to be impermeable and perfectly deformable; therefore, we can think in terms of a flow within a channel, the geometry of which may change in time, although its width (measured parallel to the y-axis) is independent of time. Currently, the flow is computed only within a portion of the channel limited by two lines, parallel to the y-axis (AA and DD), which should be considered as permeable. Such artificial boundaries are not essential. Using a suitable stretching of coordinates, the computational region could be extended to infinity in both directions. We prefer to make use of artificial boundaries for two reasons:

    1) the number of mesh points can be reduced, and

    2) different flow conditions at the inlet and outlet of the computational region can be simulated. Two boundary conditions are needed at the inlet surface. There, we prescribe the total temperature θ° and the flow angle σ, constant along the surface. One boundary condition is needed at the outlet surface. To begin with, we discuss the consequences of a simple choice of downstream boundary conditions, that is, prescribing the static pressure. In what follows, it will be shown that such a choice may give rise to ambiguities in problem i). It will also be shown how uniqueness of the solution may be restored by a different choice of a downstream boundary condition.

The inlet is considered fixed in time (AA does not change), whereas DD can slide upwards and downwards, maintaining a constant pitch.

The flow repeats itself periodically in the y-direction; the period is the pitch of the cascade.

Let y_1 and y_2 be the y-coordinates of the lower and upper wall of the channel, respectively. Therefore,

$$y_1 = y_1(x,t), \quad y_2 = y_2(x,t)$$

The computational grid is defined by constant values of X and Y in the transformed set of coordinates:

$$X = x$$

$$Y = (y-y_1)/(y_2-y_1) \tag{1.1}$$

$$T = t$$

As y_1 and y_2 vary with t, the grid points slide along their X=constant lines. Consequently, the length of the chord of the blades varies with time, and the solidity of the cascade cannot be prescribed a priori, but it will result as a part of the solution.

For simplicity, the design data are prescribed as functions of the x-coordinate, instead of a curvilinear coordinate along the camber line; the restriction, however, can be easily lifted.

By normalizing the flow properties to reference values, the equations of motion for a two-dimensional, compressible, inviscid, isentropic flow are

$$a_t + ua_x + va_y + \delta a(u_x + v_y) = 0$$

$$u_t + uu_x + vu_y + aa_x/\delta = 0 \qquad (1.2)$$

$$v_t + uv_x + vv_y + aa_y/\delta = 0$$

with $\delta = (\gamma-1)/2$. In the (X,Y)-frame:

$$a_T + ua_X + Aa_Y + \delta a(u_X + u_Y Y_x + v_Y Y_y) = 0$$

$$u_T + uu_X + Au_Y + a(a_X + a_Y Y_x)/\delta = 0 \qquad (1.3)$$

$$v_T + uv_X + Av_Y + aa_Y Y_y/\delta = 0$$

where

$$A = Y_t + uY_x + vY_y$$

$$Y_t = -Y_y[y_{1t} + Y(y_{2t}-y_{1t})]$$

$$Y_x = -Y_y[y_{1x} + Y(y_{2x}-y_{1x})] \qquad (1.4)$$

$$Y_y = 1/(y_2-y_1)$$

Following [9], we rewrite (1.3) as follows:

$$a_T = .5\delta(f_1+f_2+f_4+f_5+f_6+f_7+f_8)$$

$$u_T = .5(f_2-f_1+f_8-f_7) \qquad (1.5)$$

$$v_T = .5(f_5-f_4+2f_3)$$

where

$$f_j = -\lambda_j R_{jX} \qquad (j=1,2,3)$$

$$f_j = -\lambda_j R_j Y \qquad (j=4,5,6,7,8)$$

and

$$\lambda_1 = u - a, \quad \lambda_2 = u + a, \quad \lambda_3 = u, \quad \lambda_4 = A - aY_y$$

$$\lambda_5 = A + aY_y, \quad \lambda_6 = A, \quad \lambda_7 = A - aY_x, \quad \lambda_8 = A + aY_x$$

$$R_1 = a/\delta - u, \quad R_2 = a/\delta + u, \quad R_3 = v \qquad (1.6)$$

$$R_4 = a/\delta - v, \quad R_5 = a/\delta + v, \quad R_6 = -2a/\delta, \quad R_7 = R_1, \quad R_8 = R_2$$

The form (1.5) of the equations of motion is the result of three linear combinations of four compatibility equations on four characteristic surfaces. Each compatibility equation contains derivatives computed along two lines on a characteristic surface, viz, the bicharacteristic, along which signals propagate, and another line. The linear combinations above eliminate all terms not related to bicharacteristics or the particle path. Therefore, all f_j's express convections of a sort, and are correctly approximated using "upwind" differences. See in Fig. 1.2 a grid point and the projection of the characteristic conoid having its apex at the grid point. It is easy to see that the quantities λ_j, defined above, are the contravariant components of the velocity of propagation along the four bicharacteristics and the particle path, shown in Fig. 1.2.
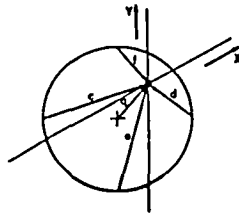

Fig. 1.2

1.2. Treatment of moving boundaries

We consider three sets of design data, as follows:

    i) the distribution of thickness $\tau(x)$ and of pressure jump between the two sides of the blades, $\Delta p(x)$,

    ii) the distribution of thickness $\tau(x)$ and of pressure along one side of the blades, $p(x)$,

    iii) the distribution of pressure along both sides of the blades.

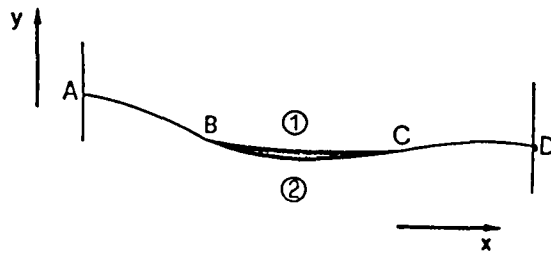We will describe the treatment of boundaries separately for each of the cases above.

Fig. 1.3

i) If $\tau(x)$ and $\Delta p(x)$ are given

Since the flow is periodic, the upper and lower boundaries of Figs. 1.1 can be reduced to a single boundary for a single blade, as in Fig. 1.3. Note that the upper part of the ABCD line in Figs. 1.1 is the lower boundary in Fig. 1.3, and vice versa.

The arcs, AB and CD are deformable and impermeable interfaces, across which the pressure is continuous but the tangential velocity component may be discontinuous. In formulating the boundary conditions, the whole ABCD arc can be treated homogeneously. The interfaces can be considered as surfaces of blades for which a vanishing thickness and a vanishing pressure jump are prescribed. With such convention in mind, we proceed to describe the technique for any blade surface.
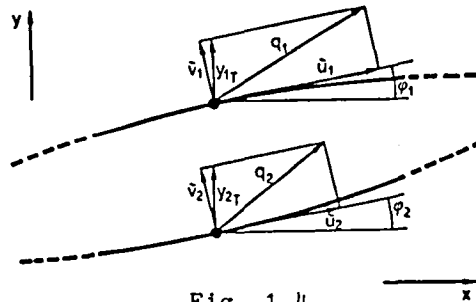
Fig. 1.4

In Fig. 1.4 we show two grid points on two different sides of the blade, at the same abscissa. The velocity vector is decomposed along the tangent and the normal to the blade at each point. Since the blade is impermeable, the two flow velocities and the blade velocity must have the same normal component. From Fig. 1.4 we see, thus, that

$$y_{1t} = \tilde{v}_1/N_1, \qquad y_{2t} = \tilde{v}_2/N_2 \qquad (1.7)$$

where $N_1 = \cos \phi_1$, $N_2 = \cos \phi_2$. In addition, the thickness is constant in time; therefore,

$$y_{1t} = y_{2t} \qquad (1.8)$$

- 8 -

The pressure jump is also constant in time; consequently, for an isentropic flow,

$$a_{1t} = a_{2t}(a_2/a_1)^{\eta} \tag{1.9}$$

where $\eta=(\gamma-1)/(\gamma+1)$. Equations (1.8) and (1.9) are the required boundary conditions.

In the spirit of [8] and [9], the computation at the boundary is performed as follows. A certain number of f_j's cannot be evaluated at boundary points since they express signals propagating towards the interior of the flow field. Such terms are considered as unknowns in (1.5) and must be evaluated using the boundary conditions. At the two boundary points shown in Fig. 1.4, there are four unknowns of this kind:
on the lower side, f_{4L} and

$$f_{7L} \quad \text{if} \quad y_{2x}>0, \qquad f_{8L} \quad \text{if} \quad y_{2x}<0$$

on the upper side, f_{5U} and

$$f_{8U} \quad \text{if} \quad y_{1x}>0, \qquad f_{7U} \quad \text{if} \quad y_{1x},0$$

where the subscripts L and U refer to the lower side and the upper side of the boundary, respectively. We dispose of two boundary conditions, Eqs. (1.8) and (1.9). Therefore, we need two additional equations. Such a difficulty is produced by the non-orthogonality of the grid [16] and it is not related to the discretization process. Any arbitrary fixing of the difficulty based on some formal manipulation of the finite difference equations (for example, approximation of certain derivatives from the "wrong" side, or extrapolations of values to fictitious points outside the boundary) has a very high probability of being incorrect, thus acting as a source of errors at every computational step. The missing equations must, indeed, describe some physical fact. Here, it will suffice to observe that the momentum equation along the boundary does not require Y-derivatives [9] to determine $\tilde{u}_{1T}$ and $\tilde{u}_{2T}$, hence

$$y_{1x}(f_{5U}-f_{4U}) + f_{8U} - f_{7U} = 0$$
$$y_{2x}(f_{5L}-f_{4L}) + f_{8L} - f_{7L} = 0 \tag{1.10}$$

These equations are identically satisfied if all finite differences are replaced by partial derivatives. In the computational code, (1.10) are used to close the set of boundary conditions. Details can be found in [9]. Specifically, if $y_{1x}>0$ and $y_{2x}>0$, the boundary conditions are expressed by

$$f_{5U} - f_{8U}y_{1x} - f_{7L}y_{2x} + f_{4L} = Q_1$$
$$f_{5U} + f_{8U} - f_{7L} - f_{4L} = Q_2 \tag{1.11}$$

$$f_{5U}y_{1x} + f_{8U} = Q_3$$

$$f_{4L}y_{2x} + f_{7L} = Q_4$$

where the right-hand sides are computed using information from the interior of the flow field:

$$Q_1 = f_{4U} - 2f_{3U} + y_{1x}(f_{2U} - f_{1U} - f_{7U}) + 2u_U y_{1tx} +$$

$$+ f_{5L} + 2f_{3L} - y_{2x}(f_{2L} - f_{1L} - f_{8L}) - 2u_L y_{2tx}$$

$$Q_2 = - f_{1U} - f_{2U} - f_{4U} - f_{6U} - f_{7U} + (f_{1L} + f_{2L} + f_{5L} + f_{6L} + f_{8L})(a_2/a_1)^n$$

$$Q_3 = y_{1x}f_{4U} + f_{7U}$$

$$Q_4 = y_{2x}f_{5L} + f_{8L}$$

Once the unknowns have been evaluated from (1.11), the new velocity of the boundary points, $y_{1t} = y_{2t}$ at time $t+\Delta t$ is computed by integrating the second derivatives, $y_{1tt} = y_{2tt}$. These, in turn, are obtained by differentiating (1.7) and using (1.5):

$$y_{1tt} = y_{2tt} = .5[f_{5L} - f_{4L} + 2f_{3L} - y_{2x}(f_{2L} - f_{1L} + f_{8L} - f_{7L}) - 2u_L y_{2tx}]$$

The factor, $y_{2tx} = y_{1tx}$ is discretized using the available values of the velocities, y_{2t}. The new locations of the boundary points, y_1 and y_2, are obtained by integration of their velocities, $y_{1t} = y_{2t}$. Hence, the components, $\tilde{v}_1$ and $\tilde{v}_2$ of the flow velocity at boundary points are computed as

$$\tilde{v}_1 = y_{1t}/(1+y_{1x}^2)^{1/2}, \quad \tilde{v}_2 = y_{2t}/(1+y_{2x}^2)^{1/2}$$

where y_{1x} and y_{2x} are evaluated using a finite difference approximation from the new values of y_1 and y_2. The other velocity components, $\tilde{u}_1$ and $\tilde{u}_2$ are obtained integrating their derivatives in time; for example,

$$\tilde{u}_{1T} = .5N_1(f_{2U} - f_{1U} + f_{8U} - f_{7U}) + (1-n^2)^{1/2}f_{3U} + N_1^2 y_{1tx}\tilde{v}_1$$

Once $\tilde{u}$ and $\tilde{v}$ are obtained, the new values of u and v are easily computed from $\tilde{u}$ and $\tilde{v}$ and the new values of y_{1x} and y_{2x}.

On either side of the blade, the new values of the speed of sound, a, are evaluated using the first of (1.5).

A less cumbersome method consists of solving (1.11) and then computing u, v and a from (1.5). The blade velocities can be evaluated from (1.7). Numerical experiments, however, have shown that the more complicated method, described above, yields more accurate results.

ii) If $\tau(x)$ and $p(x)$ on one side are given

The problem is solved as described above, with the following change: The boundary condition (1.9) is replaced by the condition, $p_{1t}=0$, that is, for isentropic flows,

$$a_{1t} = 0 \qquad (1.12)$$

if, for instance, the pressure is prescribed on the upper side of the blade. Consequently, the second of (1.11) must be replaced by

$$f_{5U} + f_{8U} = Q_5 \qquad (1.13)$$

where

$$Q_5 = - f_{1U} - f_{2U} - f_{4U} - f_{6U} - f_{7U}$$

For the remaining portions of moving boundaries (the arcs AB and CD in Fig. 1.3) the calculation proceeds as in case i).

iii) If $p(x)$ is prescribed along both sides of the blade

This problem is the same as the one described in [2] for designing the walls of a duct, with some modifications required by the different numerical scheme used here. The boundary conditions have to provide that the pressure does not change in time on both sides of the blade. Therefore, the second of (1.11) is replaced by (1.13),as in case ii) above and, similarly, the first of (1.11) is replaced by

$$f_{4L} + f_{7L} = Q_6 \qquad (1.14)$$

where

$$Q_6 = - f_{1L} - f_{2L} - f_{5L} - f_{6L} - f_{8L}$$

Again, the interfaces AB and CD (Fig. 1.3) are treated as in case i).
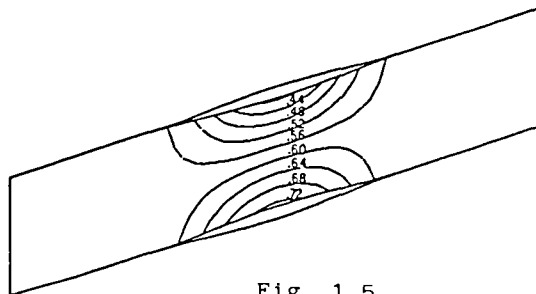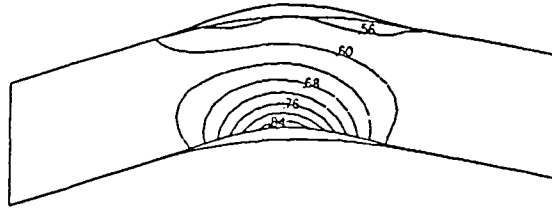

Fig. 1.5

Fig. 1.6

1.3. Numerical results

To illustrate our method and to discuss the well-posedness of the formulation, we present three sets of results: Two stable calculations for which $\tau(x)$ and $\Delta p(x)$ are prescribed, two calculations for which $\tau(x)$ and $p_1(x)$ are prescribed (one being stable and the other unstable), and an unsuccessful attempt to recompute the Hobson cascade No. 2 [4] according to formulation i).

Fig. 1.5 shows the initial configuration and Fig. 1.6 the steady solution to the inverse problem for the case corresponding to

$$\tau = .025 \; [1 - \cos(2\pi x)] \qquad (0<x<1)$$

and

$$\Delta p = .1 \; [1 - \cos(2\pi x)] \qquad (0<x<1)$$

The ratio p_e/p^0 between downstream pressure and total pressure is 0.8, the upstream slope of the velocity vector, σ is 20°, and the upstream total temperature θ^0 is 1. Both this case and the following one have been computed using 40 intervals in X and 10 intervals in Y.
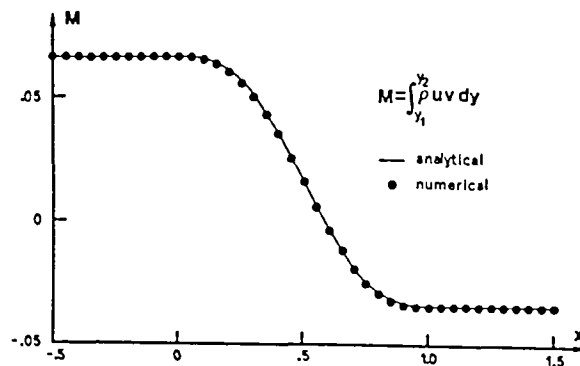
Fig. 1.7

A check on the accuracy of the computation is shown in Fig. 1.7, where the theoretical behavior of the integral of the y-momentum is compared with the numerical result. The maximum error is less than 0.1%.

The case of Fig. 1.8 has the same τ, σ, and Θ° as in the preceding case, but

$$\Delta p = .15 \ [1 - \cos(2\pi x)] \qquad\qquad (0 < x < 1)$$

and $p_e/p^\circ = 0.71$.
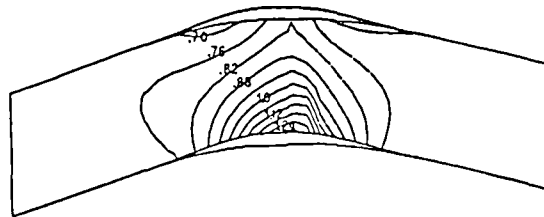
Fig. 1.8

The resulting cascade is supercritical but unchoked and shockless. It can be seen from the isomachs of Fig. 1.8 that a supersonic bubble appears on the upper side of the blade, but the lower side is entirely subsonic. The pressure cannot be discontinuous on the subsonic side; therefore, it must be continuous on the supersonic side as well, since Δp is prescribed as a continuous function of x. The method does not imply that the whole flow field is shockless, but just that the blade surface is shockless. The behavior of the isomachs of Fig. 1.8 may suggest that an imbedded shock is present inside the flow field and it vanishes at the blade wall. The method, indeed, is capable of capturing shock waves, in the sense described in [7]. The mesh resolution of Fig. 1.8 is not sufficient to provide a conclusive interpretation of the result; anyway, the possibility of designing blades that are shockless just at the wall is of great relevance from a practical viewpoint, especially in the case of supercritical compressor cascades.

In this case, as well as in the preceding one, the theoretical behavior of the y-momentum has been compared with the numerical results and the maximum error is less than 0.3%.

In the next two examples, p(x) is prescribed on one side of the blades. As mentioned above, this problem presents an ambiguity. It is not specified, indeed, whether the side along which the pressure is prescribed is the suction side or the pressure side. Our numerical experiments show that, of the two possibilities, only the one for which the pressure is prescribed on the pressure side is stable. We do not intend to say that a steady, unstable flow may exist about a cascade with rigid blades. The instability detected in the numerical

solution is related to the problem as posed here, where the blades are perfectly deformable and the data are prescribed as said above.

In the numerical experiments, the steady solution to the inverse problem i) has been used as the initial condition for the inverse problem ii). The pressure distribution on one side of the blades has been taken equal to the previously computed pressure distribution and forced to remain unchanged.
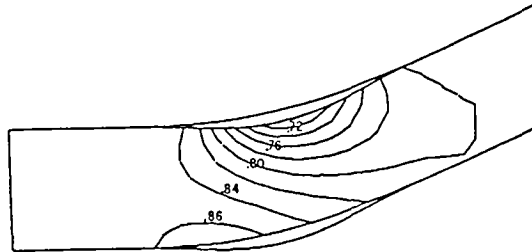

Fig. 1.9

The initial configuration and related isobars are shown in Fig. 1.9. They solve problem i) for

$$\tau = .025 \; [1 - \cos(2\pi x)] \qquad (0 < x < 1)$$

and

$$\Delta p = - .075 \; [1 - \cos(2\pi x)] \qquad (0 < x < 1)$$

with $p_e/p^0 = 0.8$, $\sigma = 0$, $\Theta^0 = 1$.

Having forced the pressure on the upper side (pressure side) of the blades to remain unchanged, 1000 more integration steps were taken. The pattern of Fig. 1.9 remains unchanged.

Then, a second computation is performed for which the initial condition, shown in Fig. 1.10, is the mirror image of Fig. 1.9. The pressure is forced again to remain unchanged on the upper side of the blade, which is now the suction side.
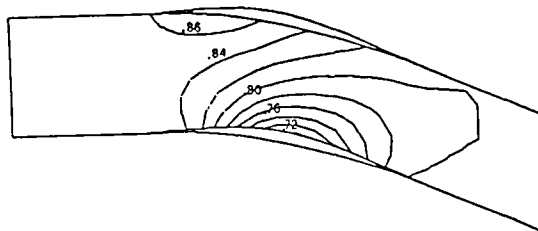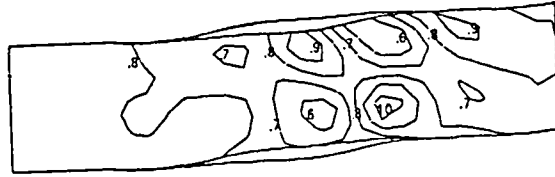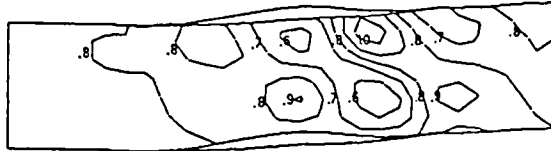

Fig. 1.10

Fig. 1.11

Fig. 1.12

After a few computational steps, minor numerical perturbations trigger a violent transient, which does not converge to a steady solution. Fig. 1.11 shows the flow field after 800 integration steps and Fig. 1.12 after 850 steps. In Fig. 1.13 the interface-and-blade velocity distributions are plotted at steps 1000 and 2000. Obviously, the flow, as computed, does not converge to a steady state.

We interpret the last two examples as follows: In the case of Fig. 1.9 the results of problem ii) perfectly agree with the results of problem i). The design pressure distribution, as assumed from a previous computation, is consistent with a well-posed problem for the pressure side. In the last example, instead, we observe two facts. First, the initial configuration is unstable for problem ii) and a transient is generated in an attempt to find a different steady solution with the upper side of the blades playing the role of a pressure side. Second, the assigned pressure distribution is inconsistent with a well-posed problem for the pressure side and the computation is unable to converge to a steady state.

Finally, Hobson's cascade No. 2 [4] and its steady flow field were adopted as initial conditions for a calculation of the first type, and we expected our computed results not to depart substantially from Hobson's. The evolution of the interface and blade lower surface, however, turns out to be very different from what we expected, as shown in Fig. 1.14. Clearly, the blade geometry tends to depart more and more from the original one. The question then arises, Why is the third calculation stable and the latter unstable, despite the apparent similarity of the procedure and of all the initial and boundary conditions? We will attempt to find an answer in
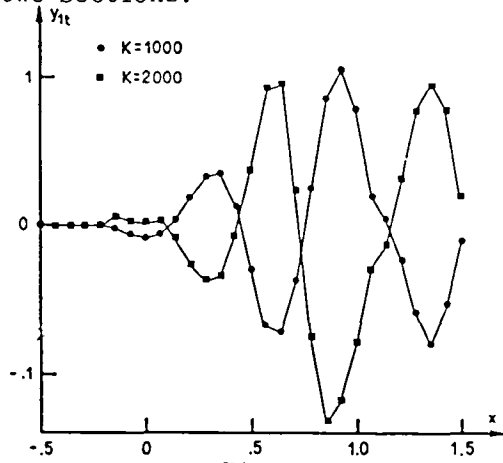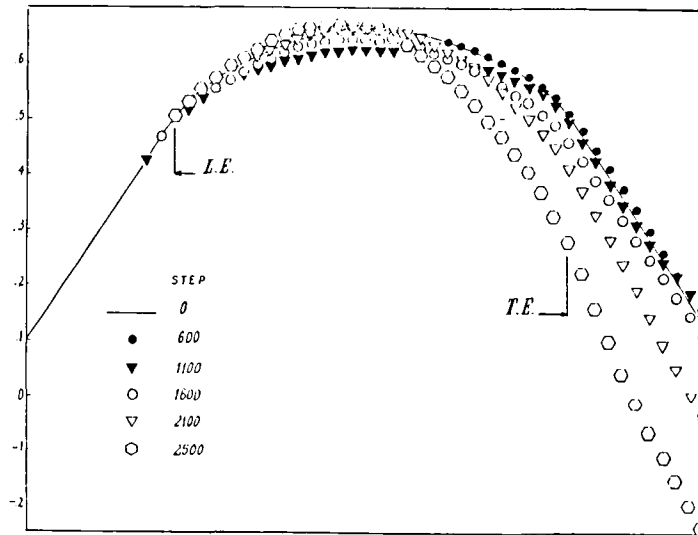
the following two Sections.

Fig. 1.13

Fig. 1.14

2. FLOW DEFLECTION AND FORCE ACTING ON A BLADE

With reference to Fig. 2.1, let us consider a cascade with inlet and outlet boundaries located sufficiently far upstream and downstream, so that the flow at such boundaries does not depend on y. Let us prescribe total temperature (Θ_i^o) and flow angle ($\circ$) upstream, and static pressure (p_e) downstream. The flow is considered isentropic. In a steady state configuration, the tangential force (F) acting on one blade is related to the upstream and downstream y-velocity components:

$$F = \dot{m} \, (v_i - v_e) \qquad\qquad (2.1)$$

where $\dot{m}$ is the mass flow through the stream channel corresponding to the pitch (s) of the cascade.
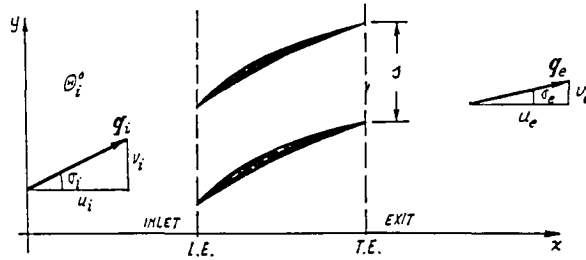

Fig. 2.1

On the other hand, F can be determined as a function of the exit flow angle, σ_e, as follows:

a) The exit velocity, q_e is a known function of $\Theta_i{}^\circ$ and p_e:

$$q_e = \sqrt{\frac{\gamma}{\delta} \, (\Theta_i{}^\circ - p_e^{2\delta/\gamma})}$$

b) Assume a value of σ_e, and let $\Sigma_e = \tan \sigma_e$,

c) The velocity components, u_e and v_e are:

$$u_e = \frac{q_e}{(1+\Sigma_e^2)^{1/2}} , \qquad v_e = \frac{q_e \Sigma_e}{(1+\Sigma_e^2)^{1/2}}$$

d) The mass flow can thus be evaluated:

$$\dot{m} = s \, u_e \, \rho_e, \qquad \text{with} \quad \rho = p_e^{1/\gamma}$$

e) p_i and the inlet velocity components are obtained by solving

$$\dot{m} = s \, \frac{q_i}{(1+\tan^2\sigma_i)^{1/2}} \, \rho_i$$

where

$$\rho_i = p_i^{1/\gamma}, \qquad q_i = \sqrt{\frac{\gamma}{\delta} \, (\Theta_i{}^\circ - p_i^{2\delta/\gamma})}$$

and $\dot{m}$ is the same as obtained in d).

- 17 -

f) Now the force F is computed, according to (2.1).

From a prescribed set of values for $\theta_i^{\,o}$, σ_i, and p_e, one can compute $F(\sigma_e)$. This relationship is plotted in Fig. 2.2. We see that F vanishes for three values of σ_e. At $\sigma_e = \pm 90^{\circ}$, because u_e and, consequently, $\dot{m}$, vanish. In these two points, the blades are so deflected at the trailing edge, that the flow has no axial velocity component. In addition, F vanishes for $\sigma_e = \sigma_i$, that is, when the blade does not deflect the flow. The force is positive when $\sigma_e < \sigma_i$, and vice versa.
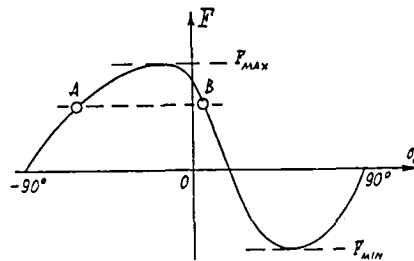
Fig. 2.2

Assume now that the inverse problem has to be solved with a set of boundary conditions ($\theta_i^{\,o}$, σ_i and p_e) and a prescribed distribution of lift over one blade ($\Delta p(x)$). On the basis of the previous considerations, two different geometries of the blade may satisfy the problem, or none. The force F results as

$$F = \int \Delta p(x) dx$$

with the integral carried over the x-axis between leading and trailing edge. If $F > F_{max}$ or $F < F_{min}$, no solution exists, but if $F_{min} < F < F_{max}$, two different cascades may be obtained, providing the same force (such as A and B, for example). The same force, thus, may be balanced, according to (2.1), by a lower mass flow and a larger deflection at point A, or by a higher mass flow and a smaller deflection at B. However, if we consider the exit boundary condition as in the previous Section, only the configuration described by point B can be reached. Let us, indeed, consider a rigid cascade providing an exit angle, σ_e, slightly smaller than $(\sigma_e)_A$, and a steady flow through it, which acts on the blades with a force slightly smaller than F_A. Let us now increase the pressure jump of this initial configuration so that the force reaches the value F_A and, at the same time, let the blade move to adjust itself to the new condition. Since F_A is larger that the initial force, the curvature of the blade

must increase and σ_e decreases, instead of increasing towards $(\sigma_e)_A$.
Thus, the blade geometry tends to move farther and farther away from
A. The opposite motion of the blade occurs if the initial value of
σ_e is slightly larger than $(\sigma_e)_A$, and the force, originally greater
than F_A, is decreased. In this case, however, the geometry of the
blade will eventually reach point B. In conclusion, B represents a
stable configuration and it is the only one which can be reached us-
ing the numerical procedure and the exit boundary condition, as for-
mulated above. Do the cascade shown in Fig. 1.8 and the Hobson cas-
cade belong to geometries of type A or B? Their curves, $F(\sigma_e)$, ob-·
tained for the values of $\theta_i°$, σ_i and p_e prescribed in Section 1, are
plotted in Fig. 2.3, where the curve labeled (1) refers to Fig. 1.8
and the one labeled (2) refers to the Hobson cascade. It is in-
teresting to see that the case of Fig. 1.8 is of the B-type, whereas
the Hobson cascade is of the A-type. It is now clear why the
geometry of Fig. 1.8 is very stable, and why we have not been able to
get a stable configuration for the Hobson cascade, even if the compu-
tation was started near the desired solution. In conclusion, the
Hobson cascade cannot be obtained, unless we modify the formulation
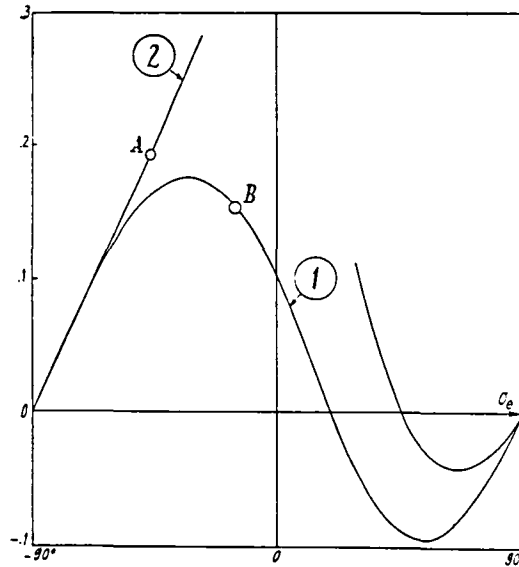of the inverse problem.

Fig. 2.3

3. ONE-DIMENSIONAL APPROACH

For an easier understanding of the conclusions of Section 2, we
will resort to a one-dimensional analysis.

The actual cascade is composed of blades of finite thickness, spaced
apart by a finite pitch. Let us replace it by a cascade of blades of
vanishing thickness, infinitely close to one another. Consequently,

all y-gradients vanish. Instead of prescribing the pressure jump distribution ($\Delta p(x)$) over a single blade, we must prescribe a force field per unit volume (f^y) along x, acting along the y-axis.

The equations of motion, formerly written as in (1.2), become

$$a_t + ua_x + \delta au_x = 0$$

$$u_t + uu_x + \frac{a}{\delta} a_x + \frac{f^x}{\rho} = 0 \qquad (3.1)$$

$$v_t + uv_x + \frac{f^y}{\rho} = 0$$

Here f^x represents the x-component of the force per unit volume. Because of the assumption of inviscid flow, the total force,

$$\mathbf{f} = f^x \, \mathbf{i} + f^y \, \mathbf{j}$$

is, at each point and at any time, perpendicular to the instantaneous shape of the blade, as shown in Fig. 3.1. So, while f^y is prescribed as a constant in time, f^x will change, during the transient, as the slope (b_x) of the blades varies:

$$f^x = - b_x \, f^y$$

Eqs (3.1) then become:

$$a_t + ua_x + \delta au_x = 0$$

$$u_t + uu_x + \frac{a}{\delta} a_x - \frac{b_x f^y}{\rho} = 0 \qquad (3.2)$$

$$v_t + uv_x + \frac{f^y}{\rho} = 0$$

Finally, the blade moves locally with the velocity, b_t defined by:

$$b_t = - ub_x + v \qquad (3.3)$$

Eqs (3.2) can be integrated in time, after having been rearranged in the proper form, as done in Section 1 (see Eqs 1.5). Once u and v are known, b_t may be evaluated and a new geometry of the blade may be predicted.

We may now proceed to some numerical experiments. Let us consider a cascade with the following set of boundary conditions: $\theta_i^\circ = 1$; $\sigma_i = 20^\circ$; $p_e = 0.9$. The curve $F(\sigma_e)$ for this case is plotted in Fig. 3.2. We assume the following distribution of f^y over the blade:
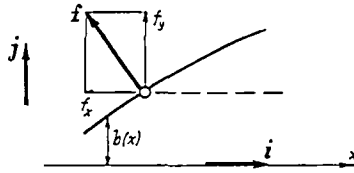
Fig. 3.1

$$f^y = 0 \qquad (0 < x < x_{l.e.}, \quad x_{t.e.} < x < 1)$$

$$f^y = 0.1238 \left[1 - \cos 2\pi \, \frac{x - x_{l.e.}}{x_{t.e.} - x_{l.e.}} \right] \qquad (x_{l.e.} < x < x_{t.e.}) \tag{3.4}$$

The force (per unit length along y) is:

$$F = \int f^y dx = 0.1238$$

The two possible configurations for the blade, corresponding to this force, are denoted by points A and B ($\sigma_{eA} = -49.28°$ and $\sigma_{eB} = -20°$). Their geometries can be easily found. At any x, the relation between v and f^y, the conservation of mass and total enthalpy yield the following three equations for the three unknowns, v, u and p:

$$v = v_i + \frac{1}{\dot{m}} \int_o^x f^y dx$$

$$u\,\rho = \dot{m} \qquad (\rho = p^{1/\gamma}) \tag{3.5}$$

$$p^{2\delta/\gamma} + \frac{\delta}{\gamma} (u^2 + v^2) = 1$$

where $\dot{m}$ is known. From u and v, the slope of the blade is obtained at each abscissa, x: $b_x = v/u$, and the blade geometry, b(x) follows, by numerical integration.

Let us consider first the cascade related to point B on Fig. 3.2. Its shape is reported in Fig. 3.3 as the curve labeled "K=0". We assume this geometry as the initial condition of a time-dependent computation, by letting the blade move and not changing the force. In the first integration steps the blade moves slightly and then it gets stabilized. The geometry at K=1000 is shown in Fig. 3.3. The slight differences between the geometries labeled K=0 and K=1000 are due to the different b(x) obtained through the integration following (3.5) and by the numerical time-dependent solution. The same stable result is reached if one starts from a geometry slightly different from the correct one.
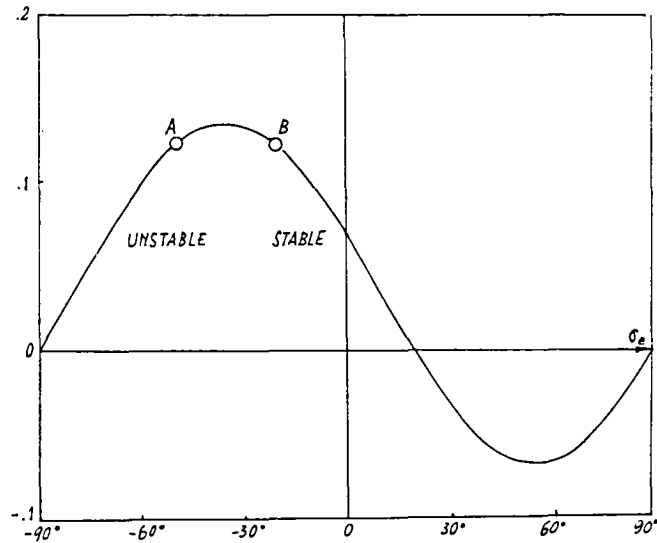
- 21 -

Fig. 3.2

We consider now the cascade related to point A. Its shape is given by the middle line in the set shown in Fig. 3.4. Once more, starting from this initial condition, we perform a time-dependent computation letting the blade move and keeping the force unchanged. As shown in Fig. 3.5, the blade tends first to move slightly down-wards, seems to get stabilized there, but at K=600 starts to move up-wards until it reaches another stable configuration, which is the one corresponding to point B. If the computation starts from the geometry shown by the upper line in Fig. 3.4, the behavior is similar to the one shown in Fig. 3.5, but the convergence to point B is even faster, as shown in Fig. 3.6.

Finally, assuming the lower line of Fig. 3.4 as the initial shape, we find that the blade moves as shown in Fig. 3.7 and the com-putation blows up. Let us point out that the behavior of the latter numerical experiment (Fig. 3.7) is very close to the degenerative process shown in Fig. 1.14 for the Hobson cascade.

In order to succeed in obtaining a geometry of the A-type, one should try to make the function $\sigma_e(F)$ single valued. All difficul-ties, indeed, seem to arise from the fact that different mass flows can provide the same force with different deflections. To achieve our goal, we replace the downstream boundary condition (constant static pressure p_e) by an exit surface modeled in the spirit of Ref. 17. As shown in Fig. 3.8, a discontinuity is located at the exit boundary, which simulates a guide forcing the flow to be discharged to the right at the prescribed static pressure, p_{ex}, and with the given angle, σ_{ex}. The flow coming onto the discontinuity (u_e, v_e, p_e) will be determined by assuming that mass flow and total
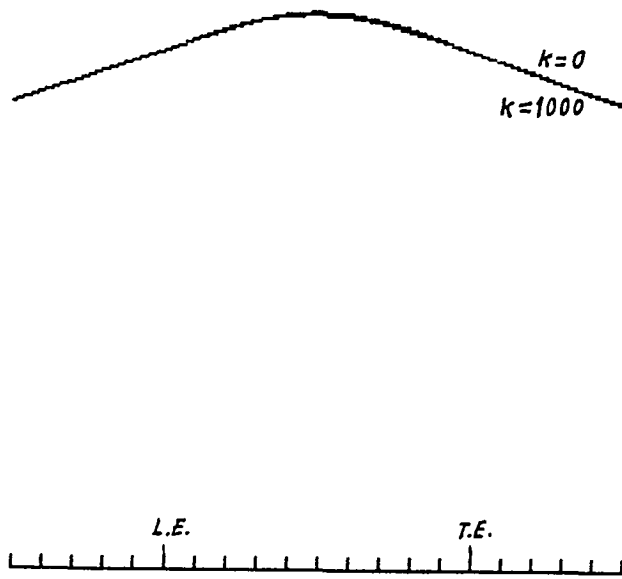
k=0
k=1000

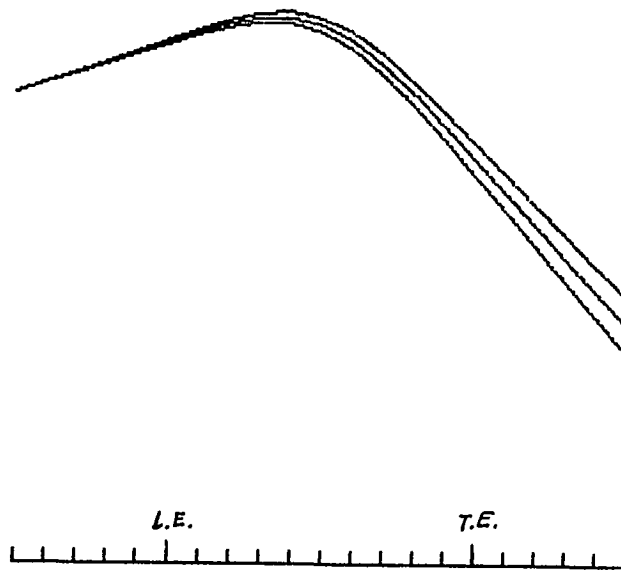L.E.   T.E.

Fig. 3.3

L.E.   T.E.

Fig. 3.4

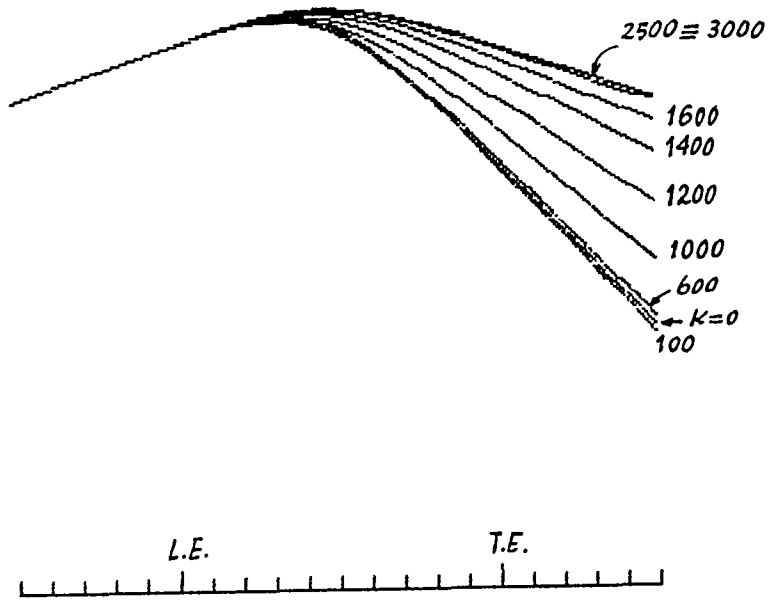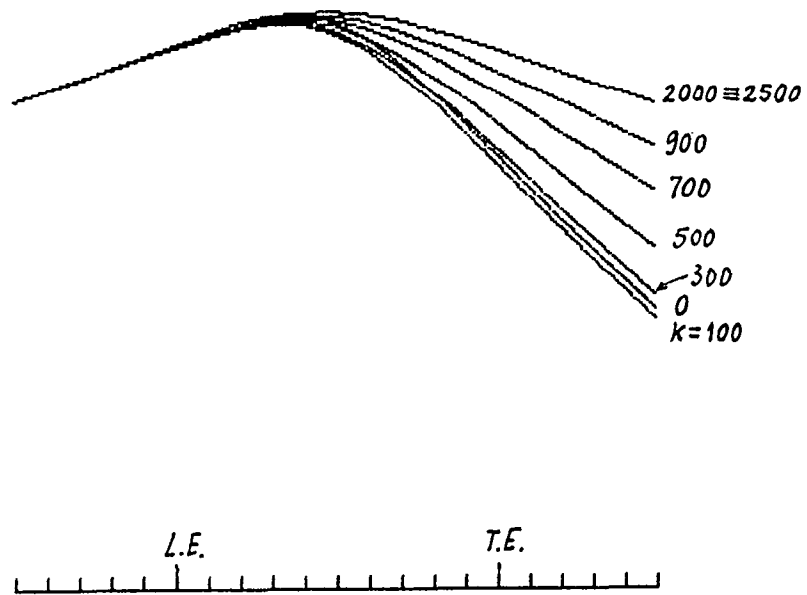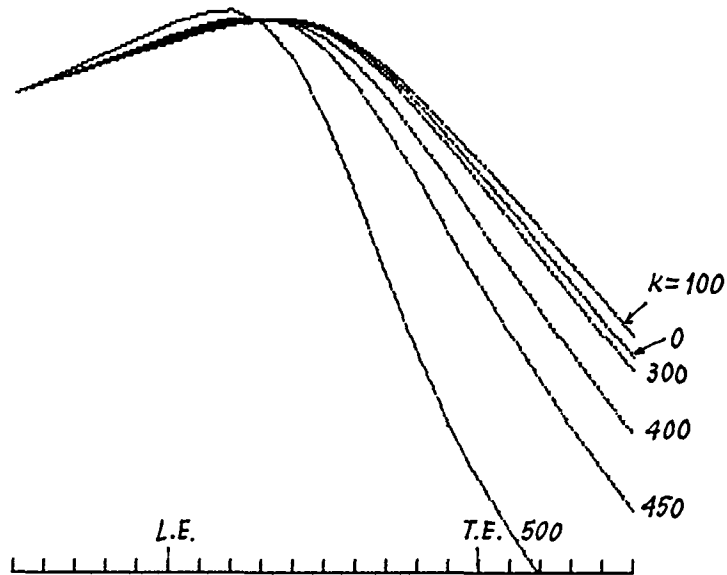Fig. 3.5

Fig. 3.6

Fig. 3.7

pressure are the same on both sides of the discontinuity:

$$\rho_e u_e = \rho_{ex} u_{ex}$$

$$\rho_e = p_e^{1/\gamma} , \qquad \rho_{ex} = p_{ex}^{1/\gamma}$$

$$p_e^{2\delta/\gamma} + \frac{\delta}{\gamma} (u_e^2 + v_e^2) = p_{ex}^{2\delta/\gamma} + \frac{\delta}{\gamma} (1+\tan^2\sigma_{ex}) u_{ex}$$

Now we can prescribe a set of boundary conditions, $\Theta_i{}^{\circ}$, σ_i, p_{ex}, σ_{ex}, and a new relationship, $F(\sigma_e)$ can be found:

a) From p_{ex} and σ_{ex}, the mass flow is computed:

$$\dot{m} = \rho_{ex} \frac{q_{ex}}{(1+\tan^2\sigma_{ex})} \qquad (q_{ex} = \sqrt{\frac{\gamma}{\delta} (p_e{}_o^{2\delta/\gamma} - p_{ex}^{2\delta/\gamma})}$$

b) Using (3.5), u,v and p are computed at all x-locations; in particular, we obtain u_e, v_e, p_e (and σ_e = arctan (v_e/u_e)) at the exit.

The function, $F(\sigma_e)$ is now monotonic, as shown in Fig. 3.9. The curve is limited by two points, M and N. For $\sigma_e<\sigma_{eM}$ and $\sigma_e>\sigma_{eN}$ it is no longer possible to maintain the same mass flow required by p_{ex} and σ_{ex}. If a force is prescribed, such that $F_M<F<F_N$, there is only one acceptable geometry which can be shown to be stable, using an argu-
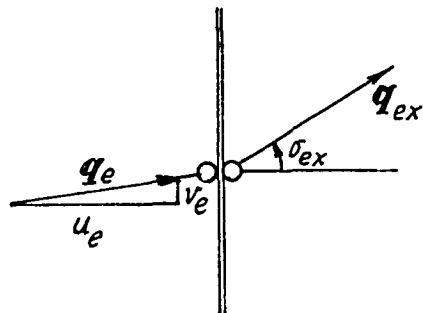
- 25 -

Fig. 3.8

ment similar to the one employed above. Our conclusions can be test-
ed numerically. In particular, if we perform the computations with
$\Theta_i^{\,o}=1$, $\sigma_i=20^o$, $F=0.1238$ and $\sigma_{ex}=-20^o$ or $\sigma_{ex}=-49.28^o$, which
correspond to the two points A and B of Fig. 3.2, we are able to
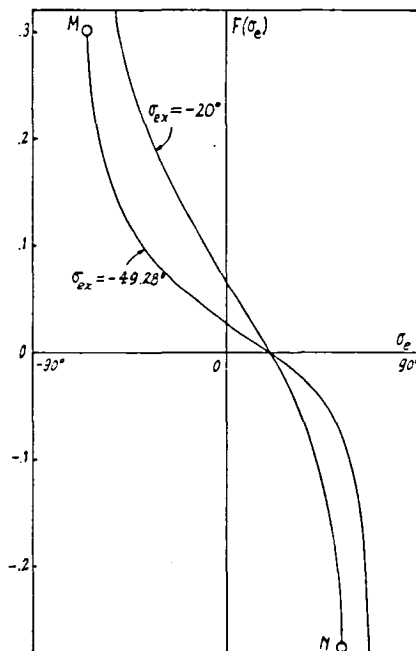predict both shapes very well and both results are perfectly stable.
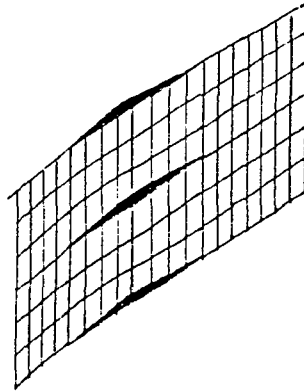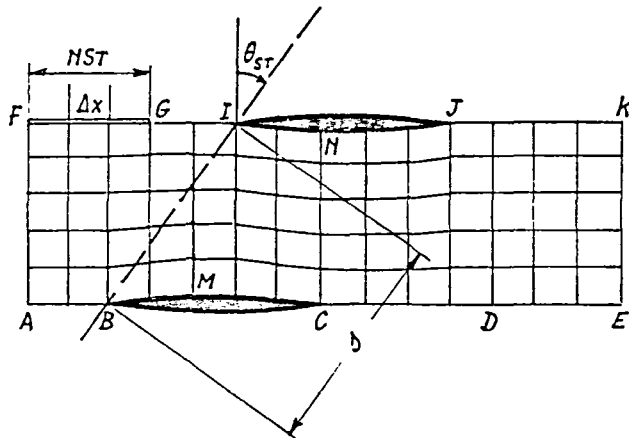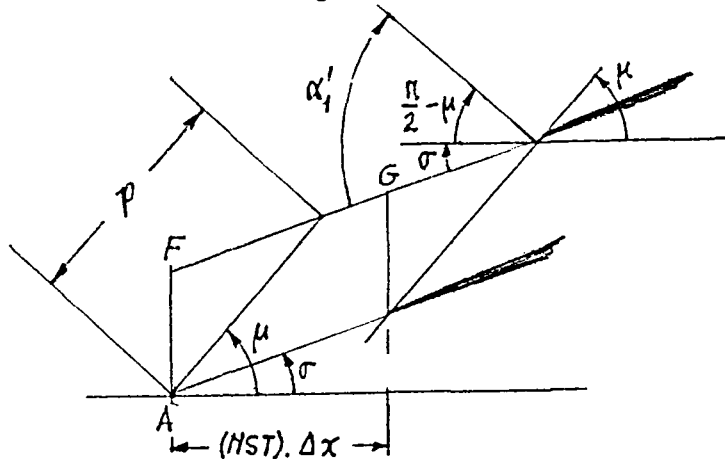

Fig. 3.9

Fig. 4.1

Fig. 4.2

Fig. 4.3

4. DESIGN OF CASCADES WITH HIGH STAGGER

If the projected cascade turns out to have a high stagger, the H-grid which we have been using so far will become very skewed, as shown in Fig. 4.1. Orthogonal grids are known to provide the highest degree of accuracy, and it is generally advisable to keep the computational grid as close to orthogonality as possible. A grid such as the one shown in Fig. 4.2 is better suited for numerical work than the grid shown in Fig. 4.1. The upper blade is shifted with respect to the lower one by a number (NST) of intervals, each of a length Δx, in the positive x-direction. Periodicity is provided by making points A,B,C and D correspond to points G,I,J and K, respectively. Periodicity conditions are imposed on AB and GI and on CD and JK. The prescribed thickness and the jumps in pressure are applied to correspondingly shifted points (for example, M and N). The inlet (AF) and outlet (EK) are treated as explained in the previous Sections. In particular, the total temperature ($\Theta_i{}^\circ$) and the flow angle (σ) are prescribed at the inlet and the static pressure (p_e) at the outlet. Points on the segment FG (except G) near the inlet and points on DE (except D) at the outlet have no correspondence with other points. The segment, FG is considered as a solid wall, having the prescribed flow direction (σ) at the inlet. The segment, DE is assumed as a flexible wall, which will adapt its shape in order to maintain a static pressure equal to p_e. Point G corresponds to A, and point D to K. The inlet blade angle, α_1', as shown in Fig. 4.3, is obtained as

$$\alpha_1' = \frac{\pi}{2} + \sigma - \arccos \frac{(NST)\,\Delta x}{p}$$

once the pitch, p is prescribed. Different inlet blade angles may be simulated by properly adjusting three parameters:

1) the value of (NST), which defines a discrete shifting of the grid points of the upper blade with respect to the corresponding points of the lower blade,
2) the value of Δx, which is determined by the number of points over the blade of a prescribed length, and
3) the inlet flow angle.

The freedom in choosing such parameters allows different final stagger angles of the cascade to be simulated.

A typical result of the design procedure with the grid described above is shown in Fig. 4.4.
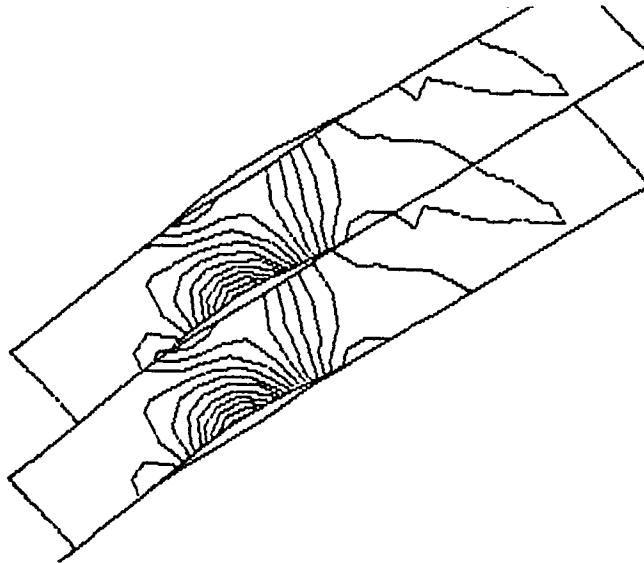
Fig. 4.4

REFERENCES

1. Zannetti, L., Transonic flow field in two-dimensional or axisymmetric convergent nozzles, Proc. 2nd GAMM-Conf. on Num. Meth. in Fluid Mech., DFLVR, Köln, October 1977, pp. 255-262

2. Zannetti, L., Time dependent method to solve the inverse problem for internal flows, AIAA J., 18, July 1980, pp. 754-758

3. Zannetti, L., Time dependent computation of the Euler equations for designing 2-D cascades, including the case of transonic shock free design, 1983 Tokyo Int. GT Congress, Paper 83-TOKYO-16TC-54

4. Hobson, D.E., Shock free transonic flow in turbomachinery cascades, Cambridge U. Eng. Dept. Report CUED/A Turbo/TR 65, 1974

5. Novak, R.E., and Haymann-Haber, G., A mixed flow cascade passage design based on power series expansion, ASME Rep. 82-GT-121

6. Moretti, G., The λ-scheme, Comp. and Fluids, 7, Sept. 1979, pp. 191-205

7. Zannetti, L., and Colasurdo, G., Unsteady compressible flow: A computational method consistent with the physical phenomena, AIAA J., 19, July 1981, pp. 852-856

8. Zannetti, L., and Moretti, G., Numerical experiments on the leading edge flow field, AIAA J., ft B 20, Dec. 1982, pp. 1668-1673

9. Moretti, G., and Zannetti, L., A new, improved computational technique for twodimensional unsteady flow, AIAA J., 22, June 1984, pp. 758-765

10. Meauze, G., An inverse time marching method for the definition of cascade geometry, ASME Paper 81-GT-167

11. Thompkins, W.T., and Sia Shing Tong, Inverse design calculation for non potential flow in turbomachinery blade passages, J. Engr. for Power, 104, pp. 281-285

12. Volpe, G., and Melnik, R.E., The roe of constraints in the inverse design problem for transonic airfoils, AIAA Paper No. 81-123, 1981

13. Lighthill, M.J., A new method of twodimensional aerodynamic design, R&M 2112, April 1945, ARC, London

14. Lighthill, M.J., A mathematical method of cascade design, R&M 2104, June 1945, ARC, London

15. Moretti, G., and Pandolfi, M., Critical study of calculations of subsonic flows in ducts, AIAA J., **19**, April 1981, pp. 449-457

16. Zannetti, L., Numerical treatment of boundaries in compressible flow problems, Proc. 4th GAMM-Conf. on Num. Meth. in Fluid Mech., Notes on Numerical Fluid Mechanics, Vol. 5, Oct. 1981, pp. 337-343

17. Pandolfi, M., and Zannetti, L., Some permeable boundaries in multidimensional flows, 6th Int. Conf. on Num. Meth. in Fluid Dynamics, Tbilisi 1978, Lecture Notes in Physics No. 90, Springer-Verlag, pp. 439-446.

1. Report No. NASA CR-3836	2. Government Accession No.	3. Recipient's Catalog No.
4. Title and Subtitle Inverse Design Technique for Cascades		5. Report Date November 1984
		6. Performing Organization Code
7. Author(s) Luca Zannetti and Maurizio Pandolfi		8. Performing Organization Report No. None
		10. Work Unit No.
9. Performing Organization Name and Address G.M.A.F., Inc. P.O. Box 184 Freeport, New York 11520		11. Contract or Grant No. NAS3-22772
12. Sponsoring Agency Name and Address National Aeronautics and Space Administration Washington, D.C. 20546		13. Type of Report and Period Covered Contractor Report
		14. Sponsoring Agency Code 505-31-0A (E-2275)

15. Supplementary Notes

Final report. Project Manager, Robert M. Stubbs, Fluid Mechanics and Instrumentation Division, NASA Lewis Research Center, Cleveland, Ohio 44135.

16. Abstract

A numerical technique to generate cascades is presented. The basic prescribed parameters are: inlet angle, exit pressure, and distribution of blade thickness and lift along a blade. Other sets of parameters are also discussed. The technique is based on the λ-scheme. Computed results are presented. The problem of stability of the computation as a function of the prescribed set of parameters and the treatment of boundary conditions is discussed. A one-dimensional analysis of the problem is provided, to indicate a possible way for assuring stability for any two-dimensional calculation.

17. Key Words (Suggested by Author(s)) Computational fluid dynamics Cascade design Transonic flow Inverse problem Lambda scheme	18. Distribution Statement Unclassified - unlimited STAR Category 02	
19. Security Classif. (of this report) Unclassified	20. Security Classif. (of this page) Unclassified	21. No. of pages 32	22. Price* A03

National Aeronautics and
Space Administration

Washington, D.C.
20546

Official Business
Penalty for Private Use, $300

NASA